

Reconstruction of the bulk magnon mean free path from spin Seebeck measurements in thin films

E. Chavez-Angel^{*1}, R. A. Zarate², S. Fuentes^{3, 4}, E. J. Guo^{1, 5}, M. Kläui^{1, 6} and G. Jakob^{1, 6}

¹ Institute of Physics, University of Mainz, Staudinger Weg 7, 55128 Mainz, Germany.

² Depto de Fisica, Universidad Católica del Norte, Av. Angamos 0610, Antofagasta, Chile.

³ Depto de Ciencias Farmaceúticas, Facultad de Ciencias, Universidad Católica del Norte, Antofagasta, Chile.

⁴ Center for the Development of Nanoscience and Nanotechnology, CEDENNA, Santiago, Chile.

⁵ Quantum Condensed Mater Division, Oak Ridge National Laboratory, 37830, Oak Ridge TN, USA

⁶ Graduate School Materials Science in Mainz, Staudingerweg 9, 55128 Mainz, Germany

*Corresponding author: cemigdio@uni-mainz.de

Abstract. A thorough understanding of the mean-free-path (MFP) distribution of the energy carriers is crucial to engineer and tune the transport properties of materials. In this context, a significant body of work has investigated the phonon and electron MFP distribution, however, similar studies of the magnon MFP distribution have not been carried out so far. In this work, we used thickness-dependence measurements of the longitudinal spin Seebeck effect of yttrium iron garnet films to reconstruct the bulk magnon MFP distribution. By using the experimental data reported by Guo et al. [Phys. Rev. X **6**, 031012 (2016)], we adapted the phonon MFP reconstruction algorithm proposed by A.J. Minnich, [Phys. Rev. Lett. **109**, 205901 (2012)] and apply it to magnons. The reconstruction showed that the magnon MFP distribution spreads orders of magnitude far beyond their typical averaged values.

Introduction

The continuous trend towards miniaturization of electronic components has allowed for more processing power at smaller dimensions. Consequently, large energy losses associated with the miniaturization have increased and cooling strategies have had to be developed. For this, thermoelectric devices have emerged as a promising green strategy for both cooling and energy harvesting. However, real applications are still limited by the low device efficiency and/or the toxicity of the component materials¹.

The quest for a new degree of freedom to improve the thermoelectric performance has opened up a new research area that includes the spin electron-heat interaction or spin caloritronics. Analogous to the

conventional Seebeck mechanism, the spin Seebeck effect (SSE) describes the generation of spin currents as a result of a thermal gradient (ΔT) across the material and it has been observed in metals, semiconductors and even in magnetic insulators². In the longitudinal (or cross-plane) SSE configuration the generated spin currents are injected into a normal metal (NM) top layer and are electrically detected by measuring the inverse spin Hall effect^{3,4}. This resultant voltage can be explained in terms of a thermal spin pumping caused by the temperature difference between the magnons in the ferromagnet (FM) and the electrons in the NM⁵.

Several reports have demonstrated a very long effective (or averaged) magnon mean-free-path (M-MFP) in the magnetic insulator yttrium iron garnet (YIG)⁶⁻¹⁰. Typically, the estimation of the M-MFP is extracted from the best fit of (i) the thickness-dependence of the local SSE^{7,8} or (ii) the separation-dependence of the injector-detector utilizing the nonlocal SSE^{6,9}. Despite the fact that the fitting approach shows a very good match between the models and the experiments, recent works have demonstrated that the use of a single-averaged MFP may be inadequate and carriers with different mean free paths have different contributions to the total transport properties¹¹⁻¹⁷.

Recently, Cuffe et al.¹² showed that by using the thickness-dependence of the thermal conductivity of silicon membranes it is possible to reconstruct the phonon-MFP dependence of the Si bulk thermal conductivity. Based on the work of Minnich¹³ and Yang and Dames¹⁷, they formulated an inverse problem of reconstructing the phonon-MFP distribution from the experimental measurements by using the known relation between the membrane thickness and phonon-MFP suppression. Their results not only showed very good agreement with other more complicated theoretical approaches (e.g., molecular dynamics and *ab-initio* calculations), but also, and more importantly, they demonstrated that it is possible to reconstruct the MFP distribution from the experimental data by knowing the characteristic suppression function of the system.

Inspired by this work, we present an extension of the phonon-MFP reconstruction algorithm to reconstruct the M-MFP and spin diffusion length distribution (SDL). By using the thickness-dependence of the longitudinal SSE (LSSE) on YIG films measured by Guo et al.⁸ and the different suppression functions, we demonstrate that the M-MFP shows a broad distribution in YIG.

Results and discussion

In a bulk system, it is well-known that the different scattering events introduced by phonons, impurities, defects and dislocations, to name a few contributions, are the main impediment for the different carriers that determinate the transport properties in a material. However, reducing the size of the system, the surface scattering mechanism is one additional term that has a strong influence on the transport and which alters the physical properties as compared with the bulk. Typically, the size-dependence of the transport properties has been analysed using the theory proposed by Fuchs¹⁸ and extended by Sondheimer¹⁹. While this model was originally developed to describe the in-plane electrical conductivity of metallic thin-films, it has been extended to calculate: thermal conductivity^{12,20,21}, Hall, Seebeck and Peltier coefficients²², the skin effect²³ and anisotropic magnetoresistance²⁴, among other properties. The Fuchs-Sondheimer model assumes that a fraction p of carriers is specularly reflected and $1 - p$ carriers are diffusively reflected by the surface, respectively. Considering pure diffusive scattering, i.e., $p = 0$, the transport property of the thin-film, α_{film} , can be related to the transport property of the bulk, α_{bulk} , by:

$$\alpha_{film} = \alpha_{bulk} S(\chi) \quad (1)$$

where $S(\chi)$ is the FS suppression function, $\chi = \Lambda/d$ is the Knudsen number, Λ is the bulk-MFP and d the film thickness. For the in-plane transport configuration the FS suppression function is given by:

$$S(\chi) = 1 - \frac{3}{8}\chi + \frac{3}{2}\chi \int_1^{\infty} (y^{-3} - y^{-5}) e^{-y/\chi} dy \quad (2)$$

while for the cross-plane geometry it is expressed by²⁵:

$$S(\chi) = 1 - 3\chi \left(\frac{1}{4} - \int_0^1 y^3 e^{-1/(y\chi)} dy \right) \quad (3)$$

The Knudsen number-dependence of the cross-plane FS suppression function is displayed in [Figure 1a](#).

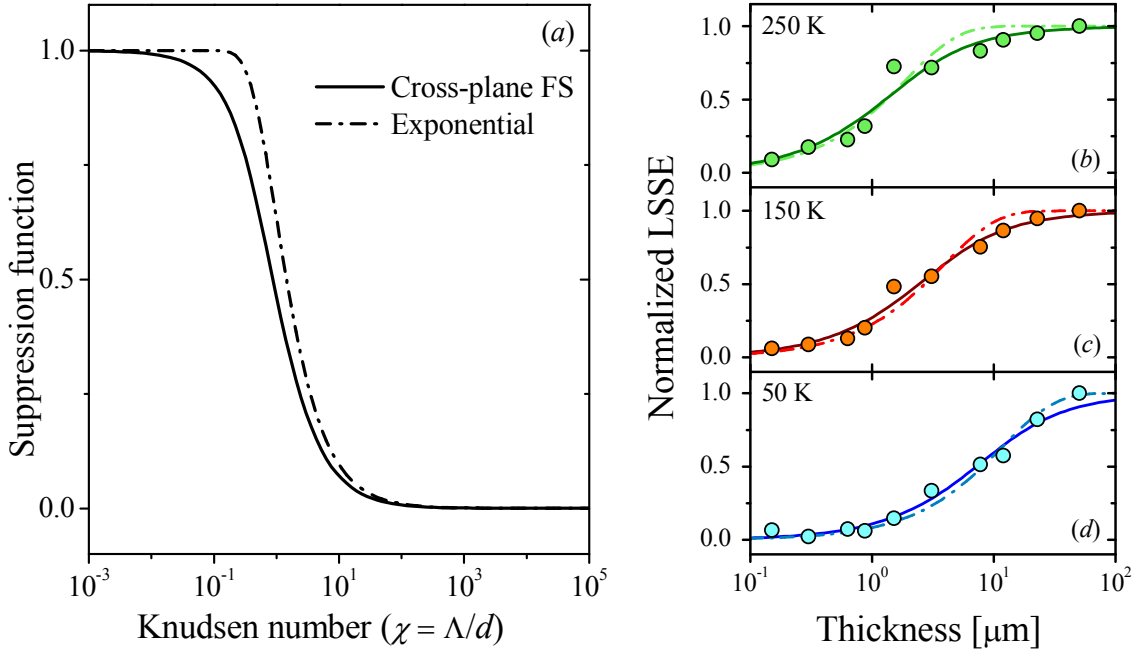


Figure 1 (a) Knudsen number (χ) dependence of cross-plane Fuchs-Sondheimer and exponential-like (Ritzmann) suppression function displayed in black-solid and red-dashed lines, respectively. (b-d) Experimental longitudinal spin Seebeck effect (LSSE) as a function of the YIG thickness measured at temperatures $T = 250$ (b), 150 (c) and 100 (d) K (green, orange and cyan dots, respectively), normalized to the thickest film sample. The experimental data were fitted by using cross-plane Fuchs-Sondheimer (solid lines) and exponential-like (dashed line) suppression functions.

For the spin Seebeck coefficient carried by magnons, Ritzmann et al.²⁶ showed that, by using an atomistic spin model with the stochastic Landau-Lifshitz-Gilbert equation as the underlying equation of motion, the thickness dependence (suppression function) of the LSSE is given by:

$$\frac{\alpha_{film}}{\alpha_{bulk}} = S(\chi) = 1 - \exp(-1/\chi) \quad (4)$$

Typically, the best fitting curves to the experimental data are used to extract an effective or averaged MFP. As an example, the best fitting curves of the LSSE in YIG films are shown in the Figure 1 (b-d). The experimental data was obtained from Ref [8] and they were normalized using the value of the thickest film sample $d = 55$ μm . It is important to mention that the exponential fitting was carried out by adjusting just the effective MFP, which is different from Ref [8] where the amplitude of the fitting was also varied, leading to small differences in the fitted values. A summary of the averaged M-MFP, Λ_{av} , for different suppression functions and at different temperatures is displayed in Table 1.

T [K]	Cross-plane FS (Eq. 3)	Exponential-like (Eq. 4)
	Λ_{av} [μm]	Λ_{av} [μm]
250	1.1	1.9
200	1.6	2.8
150	2.1	3.9
100	3.1	5.7
50	6.3	11.7

Table 1. Averaged magnon mean free path for different temperatures and suppression functions.

Despite the good match between the different models and the experiment, recent works have demonstrated that the use of a single averaged MFP maybe inadequate and carriers with different mean free paths have different contributions to the total transport properties¹¹⁻¹⁴.

Taking into account this effect, Minnich¹³ suggested a method to extract the MFP accumulation function based on a characteristic suppression function, which depends on the geometry and the experimental configuration. For the particular case of the thermal conductivity of a thin Si membrane, Cuffe et al.¹² showed that the measured thermal conductivity of a film ($\alpha_{film}(d)$) and the suppression function are related through a cumulative MFP distribution given by^{12,13}:

$$\alpha_{film}(d) = \int_0^{\infty} S(\chi) f(\Lambda) d\Lambda \quad (5)$$

$$\alpha = \frac{\alpha_{film}(d)}{\alpha_{bulk}} = \int_0^{\infty} K(\chi) F_{acc}(\Lambda) d\Lambda, \text{ with} \quad (6)$$

$$F_{acc}(\Lambda_c) = \frac{1}{\alpha_{bulk}} \int_0^{\Lambda_c} f(\Lambda') d\Lambda', \text{ and } K(\chi) = -\frac{dS(\chi)}{d\chi} \frac{d\chi}{d\Lambda} \quad (7)$$

The $F_{acc}(\Lambda_c)$ represents the fraction of transport property contribution from all the carriers with MFP less than Λ_c ¹² and $K(\chi)$ represents the computational Kernel of the integral. Then, to recover $F_{acc}(\Lambda)$ from the experimental data it is necessary to have a wide enough range of measurements at different film thicknesses. The solution of Eq. (6) is technically an ill-posed problem and, in principle, with infinite solutions. However, Minnich¹³ showed that one can discretize the integral and to impose some constraints to the F_{acc} to obtain a unique solution. These conditions are expressed in terms of a minimization problem through the Tikhonov regularization method given by:

$$\min \left\{ \|A \cdot F - \alpha\|_2^2 + \mu \|L \cdot F\|_2^2 \right\} \quad (8)$$

where $\| \cdot \|_2$ is the second-norm operator, α_i is the normalized LSSE of the i^{th} measurement, $A_{i,j} = K(\chi_{i,j}) \cdot \beta_j$ is a $m \times n$ matrix with m the number of measurements and n the discretization points of the integral, β_j is the weight of the quadrature point at $\chi_{i,j} = \Lambda_j / d_i$, F is a vector of the desired accumulation function (F_{acc}), μ is the regularization parameter to control the smoothness of F and L is a $(n-2) \times n$ tridiagonal Toeplitz matrix which represents an approximation of a second derivative operator, i.e., $L \cdot F = F_{i+1} - 2F_i + F_{i-1}$.

Finally, to numerically solve the bulk M-MFP reconstruction, we have discretized the integral of [Eq. \(6\)](#) through a trapezoid method using 50 logarithmic-spaced points with a regularization parameter $\mu = 1$ and the suppression functions defined in [Eq. \(3\)](#) and [\(4\)](#), which describe the cross-plane (longitudinal) transport. The minimization of [Eq. \(8\)](#) was performed by using CVX, a package for specifying and solving convex programs^{27,28}, and the experimental data of the LSSE in YIG films reported by Guo et al. [8].

The reconstructed bulk M-MFP for three different temperatures is shown in [Figure 3](#). The M-MPF distribution was calculated using a cross-plane Fuchs-Sondheimer and an exponential-like suppression function represented by solid and dashed lines, respectively. The solid-circles and solid-squares show the MFP of magnons which contribute 50 % to the overall LSSE in YIG.

We notice that depending on the selected suppression function the M-MFP spans different ranges. This difference is basically due to the mathematical nature of each expression. For the FS-like suppression function ([Eq. \(3\)](#)) the M-MFP ranges from ~ 0.4 - 3.9 μm , 1.1 - 7.6 μm and 1.9 - 17.3 μm for $T = 250$, 100 and 50 K, respectively, contributing between 10-90% to the overall LSSE. Whereas for the exponential-like function ([Eq. \(4\)](#)) the M-MFP shows a broader distribution spanning from ~ 0.6 - 11 μm , 1.6 - 16.6 μm and 3 - 34 μm for the same temperature values and percentages of contribution.

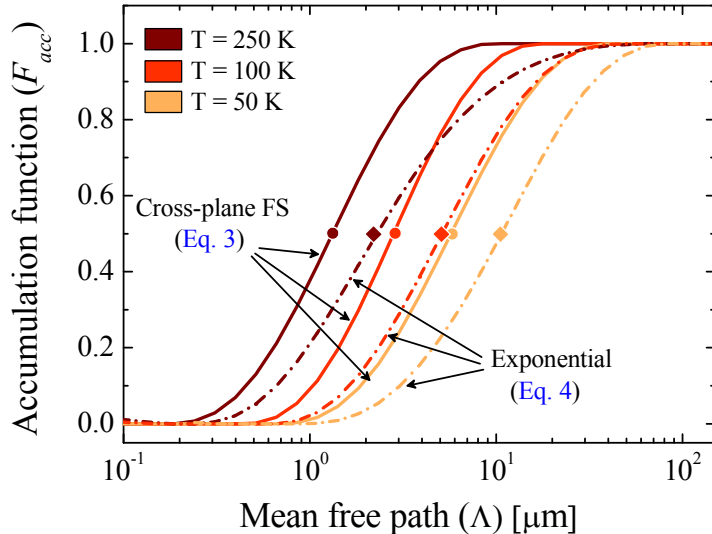


Figure 2 Reconstructed magnon MFP distribution for YIG using cross-plane Fuchs-Sondheimer (FS, solid lines) and exponential (dashed lines) reduction functions at three different temperatures $T = 250, 100$ and 50 K, respectively. The solid-circles and solid-squares represent the magnon-MFP carrying 50% of the SSE for FS and exponential reduction function respectively.

For both the FS and the exponential suppression function, we observe that the M-MFP does not show a single value and it is extended far beyond to their averaged value (see Table 1). In a similar way than phonons, MFPs longer than 1.3-2.2 μm (see the solid-circles and solid-squares in the Figure 3) contribute 50% to the total LSSE, and, as we go down in temperature, magnons with longer MFPs become more important and the MFP distribution becomes broader.

The large distribution of the M-MFP will have a strong impact on the maximum value of the LSSE at low temperatures. As it was reported by Guo et al. [8], the maximum SSE peak shows a strong dependence on the film thicknesses. It shifts to higher temperatures as the thickness decreases, disappearing completely for thickness below 1 μm . This effect indicates that magnons dissipate their energy mainly by boundary scattering, and, as a consequence, in a similar manner to phonon-transport, the boundary will impose an upper limit to the MFP. Then, the maximum of the LSSE will shift to higher temperatures, i.e., magnons with a shorter MFP, until it disappears completely in the ultra-thin film limit²⁹.

It is important to remark that the M-MFP values derived from the LSSE will be valid for this system of Pt/YIG. The LSSE is also dependent on the interface quality of NM/YIG^{7,8,30} and the thickness of NM layer³¹⁻³³. Taking into account this effect we also have calculated the spectral distribution of the spin

diffusion length (SDL) of Pt. Based on the thickness dependence of the spin Hall torque efficient, ξ , reported by Nguyen et al.³³ for Co/Pt bilayers and the functional suppression function given by³⁴:

$$\frac{\xi(d)}{\xi_{\max}} = 1 - \frac{1}{\sinh(1/\chi)}, \quad (9)$$

the SDL distribution of Pt is presented on [Figure 3](#).

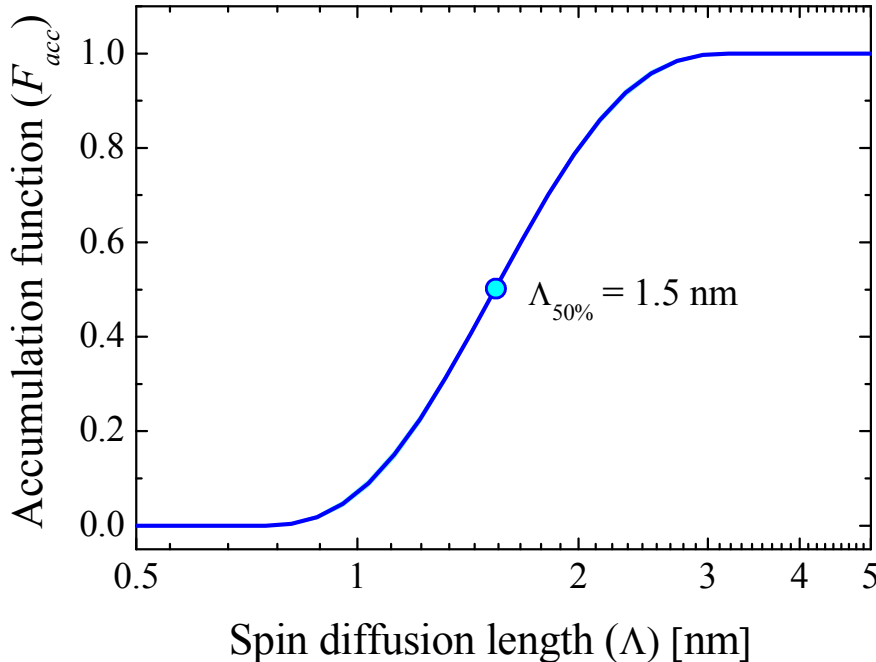


Figure 3 Room-temperature reconstructed spin diffusion length of Pt films. The reconstruction was carried out using Eq (9) and by using the thickness dependence of the spin Hall torque efficient reported in ref [33].

In contrast to the M-MFP distribution, the SDL distribution for Pt spans in a narrower region between 1.0-2.3 nm for 10 to 90% contribution. It indicates that the use of a single averaged value of the spin diffusion length is indeed a good approximation. However, this is just a first approximation and the resistivity thickness dependence also plays a role in the form of the suppression function. In this context, a deeper study of this function is needed to obtain a complete insight into the distribution of the SDL.

Conclusions

Using the experimental size-dependence of the spin Seebeck effect in YIG films and the phonon MFP-reconstruction algorithm, we showed that by an extension of this concept applied to the LSSE data, one can calculate an effective magnon MFP distributions. The reconstruction was performed using cross-plane Fuchs-Sondheimer and exponential suppression functions. Both functions showed that the M-

MFP distribution spreads a range of values (at least two order of magnitude) far beyond the averaged value. Note that this M-MFP derived from the SSE measurements will be valid for a given system consisting of NM/YIG including the specific interface and thickness of NM layer. Consequently one needs to take into account the spin-charge conversion processes at the interface and the results need to be considered as effective values valid for this system, however the numerical procedure can be applicable to any configuration. By developing spectrally independent spin charge conversion of the spin wave transmission at the interface, combined with a spectrally independent inverse spin Hall effect this analysis can provide the intrinsic M-MFP.

Additionally, using the same algorithm the distribution of the spin diffusion length was also carried out. In contrast to magnons, the spin diffusion length showed a narrow distribution, indicating that the single averaged values can be used as a good approximation in this case.

Acknowledgments

We gratefully acknowledge financial support by the Deutsche Forschungsgemeinschaft, DFG, Germany, [Grants No. Ja821/4 within SPP 1386 (Nanostructured Thermoelectric Materials) and No. Ja821/7-1 and KL1811/7-2 within SPP 1538 (Spin Caloric Transport)], the Transregional Collaborative Research Center SFB/TRR173 “Spin+X— Spin its collective environment” and the EU project InSpin [Grant No FP7-ICT-2013-612759]. R.Z.A. gratefully acknowledges financial support from ACT1204 [ANILLO DE INVESTIGACIÓN] and SF acknowledges financial support from CEDENNA FB0807. We thank Dr. John Cuffe and Dr. Ulrike Ritzmann for the valuable discussions.

References

- ¹ S. LeBlanc, Sustain. Mater. Technol. **1-2**, 26 (2014).
- ² G.E.W. Bauer, E. Saitoh, and B.J. van Wees, Nat. Mater. **11**, 391 (2012).
- ³ E. Saitoh, M. Ueda, H. Miyajima, and G. Tatara, Appl. Phys. Lett. **88**, 182509 (2006).
- ⁴ K. Uchida, S. Takahashi, K. Harii, J. Ieda, W. Koshibae, K. Ando, S. Maekawa, and E. Saitoh, Nature **455**, 778 (2008).
- ⁵ H. Adachi, K. Uchida, E. Saitoh, and S. Maekawa, Reports Prog. Phys. **76**, 036501 (2013).
- ⁶ L.J. Cornelissen, J. Liu, R.A. Duine, J. Ben Youssef, and B.J. van Wees, Nat. Phys. **11**, 1022 (2015).

⁷ A. Kehlberger, U. Ritzmann, D. Hinzke, E.-J. Guo, J. Cramer, G. Jakob, M.C. Onbasli, D.H. Kim, C.A. Ross, M.B. Jungfleisch, B. Hillebrands, U. Nowak, and M. Kläui, Phys. Rev. Lett. **115**, 096602 (2015).

⁸ E.-J. Guo, J. Cramer, A. Kehlberger, C.A. Ferguson, D.A. MacLaren, G. Jakob, and M. Kläui, Phys. Rev. X **6**, 031012 (2016).

⁹ B.L. Giles, Z. Yang, J.S. Jamison, and R.C. Myers, Phys. Rev. B **92**, 224415 (2015).

¹⁰ L.J. Cornelissen and B.J. van Wees, Phys. Rev. B **93**, 020403 (2016).

¹¹ K.T. Regner, D.P. Sellan, Z. Su, C.H. Amon, A.J.H. McGaughey, and J.A. Malen, Nat. Commun. **4**, 1640 (2013).

¹² J. Cuffe, J.K. Eliason, A.A. Maznev, K.C. Collins, J.A. Johnson, A. Shchepetov, M. Prunnila, J. Ahopelto, C.M. Sotomayor Torres, G. Chen, and K.A. Nelson, Phys. Rev. B **91**, 245423 (2015).

¹³ A.J. Minnich, Phys. Rev. Lett. **109**, 205901 (2012).

¹⁴ B. Qiu, Z. Tian, A. Vallabhaneni, B. Liao, J.M. Mendoza, O.D. Restrepo, X. Ruan, and G. Chen, Europhys. Lett. **109**, 57006 (2015).

¹⁵ B. Liao, J. Zhou, B. Qiu, M.S. Dresselhaus, and G. Chen, Phys. Rev. B **91**, 235419 (2015).

¹⁶ A. Jain and A.J.H. McGaughey, Phys. Rev. B **93**, 081206 (2016).

¹⁷ F. Yang and C. Dames, Phys. Rev. B **87**, 035437 (2013).

¹⁸ K. Fuchs, Math. Proc. Cambridge Philos. Soc. **34**, 100 (1938).

¹⁹ E.H. Sondheimer, Adv. Phys. **1**, 1 (1952).

²⁰ M. Asheghi, Y.K. Leung, S.S. Wong, and K.E. Goodson, Appl. Phys. Lett. **71**, 1798 (1997).

²¹ M. Asheghi, M.N. Touzelbaev, K.E. Goodson, Y.K. Leung, and S.S. Wong, J. Heat Transfer **120**, 30 (1998).

²² B.S. Verma and G.C. Jain, Thin Solid Films **10**, 71 (1972).

²³ G.E.H. Reuter and E.H. Sondheimer, Proc. R. Soc. A Math. Phys. Eng. Sci. **195**, 336 (1948).

²⁴ T.G.S.M. Rijks, R. Coehoorn, M.J.M. de Jong, and W.J.M. de Jonge, Phys. Rev. B **51**, 283 (1995).

²⁵ C. Hua and A.J. Minnich, J. Appl. Phys. **117**, 175306 (2015).

²⁶ U. Ritzmann, D. Hinzke, and U. Nowak, Phys. Rev. B **89**, 024409 (2014).

²⁷ M. Grant and S. Boyd, in *Recent Advances in Learning and Control*, edited by V. Blondel, S. Boyd, and H. Kimura (Springer-Verlag Limited, 2008), pp. 95–110.

²⁸ M. Grant and S. Boyd, CVX Matlab Software Disciplined Convex Programming Version 2.1 (2014).

²⁹ H. Panda, in *Nanoscience and Nanotechnology Handbook* (Asia Pacific Business Press Inc, Delhi, 2010), pp. 74–84.

³⁰ A. Aqeel, I.J. Vera-Marun, B.J. van Wees, and T.T.M. Palstra, J. Appl. Phys. **116**, 153705 (2014).

³¹ Y. Saiga, K. Mizunuma, Y. Kono, J.C. Ryu, H. Ono, M. Kohda, and E. Okuno, Appl. Phys. Express **7**, 093001 (2014).

³² D. Qu, S.Y. Huang, J. Hu, R. Wu, and C.L. Chien, Phys. Rev. Lett. **110**, 067206 (2013).

³³ M.-H. Nguyen, D.C. Ralph, and R.A. Buhrman, Phys. Rev. Lett. **116**, 126601 (2016).

³⁴ H. Kurt, R. Loloee, K. Eid, W.P. Pratt, and J. Bass, Appl. Phys. Lett. **81**, 4787 (2002).